Yeast homologues of lethal giant larvae and type V myosin cooperate in the regulation of Rab-dependent vesicle clustering and polarized exocytosis

Guendalina Rossi and Patrick Brennwald
Department of Cell and Developmental Biology, University of North Carolina at Chapel Hill, Chapel Hill, NC 27599-7090

ABSTRACT **Lgl family members play an important role in the regulation of cell polarity in eukaryotic cells. The yeast homologues Sro7 and Sro77 are thought to act downstream of the Rab GTPase Sec4 to promote soluble *N*-ethylmaleimide–sensitive factor adaptor protein receptor (SNARE) function in post-Golgi transport. In this article, we characterize the interaction between Sro7 and the type V myosin Myo2 and show that this interaction is important for two distinct aspects of Sro7 function. First, we show that this interaction plays a positive role in promoting the polarized localization of Sro7 to sites of active growth. Second, we find evidence that Myo2 negatively regulates Sro7 function in vesicle clustering. Mutants in either Myo2 or Sro7 that are defective for this interaction show hypersensitivity to Sro7 overexpression, which results in Sec4-dependent accumulation of large groups of vesicles in the cytoplasm. This suggests that Myo2 serves a dual function, to both recruit Sro7 to secretory vesicles and inhibit its Rab-dependent tethering activity until vesicles reach the plasma membrane. Thus Sro7 appears to coordinate the spatial and temporal nature of both Rab-dependent tethering and SNARE-dependent membrane fusion of exocytic vesicles with the plasma membrane.**

Monitoring Editor
Anne Spang
University of Basel

Received: Jul 7, 2010
Revised: Jan 5, 2011
Accepted: Jan 6, 2011

INTRODUCTION

Polarized vesicle transport is the product of both the directional movement of vesicles toward sites of active growth and the subsequent docking and fusion of these vesicles at specific sites of the plasma membrane. The directed movement of vesicles involves vesicle-associated motor proteins moving along microtubule or actin cytoskeletal tracks. Once delivered to the proper site, docking or tethering factors bring vesicles into close proximity of the target membrane and facilitate subsequent fusion events. The coordination of the timing and localization of each of these steps is critical to the temporal and spatial specificity of plasma membrane delivery events in eukaryotic cells (Vale, 2003; Krendel and Mooseker, 2005).

Rab guanosine 5′-triphosphatases (GTPases) are thought to play important roles in coordinating several distinct stages of exocytosis. The budding yeast *Saccharomyces cerevisiae* has been an important model system for dissecting these specific contributions (Segev, 2001; Spang, 2004; Grosshans *et al.*, 2006). In particular, during post-Golgi transport, two families of Rab GTPases, Ypt31/32 and Sec4, have been shown to function in vesicle delivery, docking, and fusion. Active (GTP-bound) Ypt31/32 is important for two initial events. First, Ypt31/32 play a role in the recruitment of the type V myosin motor Myo2 to secretory vesicles, which is required for vesicle delivery along actin cables toward sites of polarized growth (Lipatova *et al.*, 2008). Second, Ypt31/32 is necessary for recruiting Sec2, a guanine nucleotide exchange factor responsible for activating the downstream Rab GTPase Sec4 (Ortiz *et al.*, 2002). The presence of GTP-bound Sec4 on vesicles is necessary

This article was published online ahead of print in MBoC in Press (http://www.molbiolcell.org/cgi/doi/10.1091/mbc.E10-07-0570) on January 19, 2011.

Address correspondence to: Patrick Brennwald (pjbrennw@med.unc.edu).

Abbreviations used: CaM, calmodulin; FITC, fluorescein isothiocyanate; GDP, guanosine 5′-diphosphate; GFP, green fluorescent protein; GST, glutathione *S*-transferase; Ig, immunoglobulin; GTPase, guanosine 5′-triphosphatase; Mlc1, myosin light chain 1; RFP, red fluorescent protein; SNARE, soluble *N*-ethylmaleimide–sensitive factor adaptor protein receptor; tet, tetracycline; TRIC, tetramethyl rhodamine isothiocyanate; t-SNARE, target membrane SNARE; YPD, yeast peptone dextrose;

for subsequent vesicle tethering to specific sites on the plasma membrane (Salminen and Novick, 1989). The Sec15 subunit of the multiprotein exocyst complex acts as a direct effector for Sec4 and allows vesicle tethering to the target membrane through its association with members of the exocyst complex at the plasma membrane (Guo *et al.*, 1999; Boyd *et al.*, 2004).

A second effector for the Sec4 GTPase is Sro7, a yeast member of the Lgl family of tumor suppressors. Both Sro7 and its homologue, Sro77, were initially identified based on their physical association with the plasma target membrane SNARE (t-SNARE). Sec9 and, like other late-acting *sec* genes, were shown to be required for efficient post-Golgi vesicle docking and fusion (Lehman *et al.*, 1999). Biochemical and structural studies demonstrated that Sro7 has an intramolecular autoinhibited interaction with Sec9 that can be "triggered" to allow the assembly of active t-SNARE complexes to occur in a spatially and temporally restricted manner (Hattendorf *et al.*, 2007). In addition to its likely role in soluble *N*-ethylmaleimide–sensitive factor adaptor protein receptor (SNARE)-mediated fusion, Sro7 was found to have both biochemical and genetic properties consistent with a role as a direct effector for Sec4. Proteomic and biochemical analyses with purified proteins demonstrated that Sro7 binds to Sec4 in a GTP-specific manner. Moreover, overexpression of Sro7 was found to suppress a Sec4 effector domain mutant and a number of deletions in components of the exocyst complex. Taken together, this suggested a role for Sro7 in an effector pathway that functions parallel to that of the exocyst complex (Grosshans *et al.*, 2006).

Sro7 has been shown to interact physically with Myo2 (Gangar *et al.*, 2005), the type V myosin motor required for post-Golgi vesicle transport (Walch-Solimena *et al.*, 1997; Pruyne *et al.*, 1998). Myo2 consists of an N-terminal actin-binding domain, which couples ATP hydrolysis to motor activity, and a C-terminal globular tail, which binds to the vesicle cargo being transported. Within the central neck region of Myo2 lies a coiled-coil domain that is responsible for dimer formation and a light chain binding site. Recent work with myosin Va in synaptic vesicle transport has suggested that, besides their involvement in vesicle transport, type V myosin motors might also affect vesicle maturation and docking at the plasma membrane (Kogel *et al.*, 2010).

In this report we examine the role of Myo2 as both a positive and negative regulator of Sro7 function in the cell. We have mapped the site of this interaction to precise regions within Myo2 and Sro7 and show that Sro7 is recruited to sites of polarized growth through this interaction and cells defective in this interaction show loss of secretory function similar to *sro7*Δ, *sro77*Δ mutant cells. Interestingly, we also show that when the Myo2–Sro7 interaction is disrupted, cells become hypersensitive to overexpression of Sro7 and exhibit a post-Golgi vesicle clustering phenotype. We show that post-Golgi vesicle clustering induced by Sro7 resembles that induced by the other characterized effector of Sec4, Sec15. In both cases, post-Golgi vesicle clustering requires the positive action of Sec4 and is independent of downstream Sec9 t-SNARE function. This work suggests a model whereby Sro7 is recruited to post-Golgi vesicles through its interaction with Myo2. By binding to Myo2, Sro7 is kept inactive until it is delivered to sites of polarized growth, where the interaction with Myo2 is relieved, and Sec4-dependent tethering with the appropriate membrane can occur.

RESULTS

Mutations in the IQ motifs of Myo2 affect binding to Sro7 in vitro and behave like loss-of-Sro7-function mutants in vivo

A previous proteomic analysis of Sro7 (Gangar *et al.*, 2005) identified Myo2 as one of two major binding partners for Sro7 (the other being the t-SNARE Sec9). Myo2 (Figure 1A) has an N-terminal motor domain and a C-terminal globular tail region that binds to vesicles and other cargo (Johnston *et al.*, 1991; Catlett and Weisman, 1998; Schott *et al.*, 1999). The central neck region contains a coiled-coil domain that is required for dimer formation (Beningo *et al.*, 2000) and an IQ domain that is required for interaction with light chains, including myosin light chain 1 (Mlc1) and light chain–like proteins, such as calmodulin (CaM) (Stevens and Davis, 1998). In vitro binding experiments with recombinant portions of Myo2 suggested that the binding site for Sro7 appeared to reside within the Myo2 central neck region (782–990) (Gangar *et al.*, 2005). To further delineate the site of interaction within Myo2, we in vitro translated smaller elements of the Myo2 neck region that contained either the IQ domain (782–925) or the coiled-coil region (871–1204) and looked for their ability to bind to purified ProtA-Sro7 bound to immunoglobulin (Ig) G beads. The results, shown in Figure 1B, demonstrated that the IQ region alone was sufficient to yield strong binding to immobilized ProtA-Sro7 bound to IgG beads but not to control beads containing ProtA alone. The IQ domain of Myo2 is composed of six consecutive repeats of the IQ consensus sequence IQXXXRGXXXR, where X represents any amino acid (Johnson *et al.*, 1991; Bähler *et al.*, 2002). Although deletion of all six IQ motifs resulted in a myosin (*myo2-Δ6IQ*) that could still support growth (Stevens and Davis, 1998), reductions in the number of the IQ motifs were shown to affect the motor function of Myo2 negatively and result in a decrease in post-Golgi vesicle transport velocity (Schott *et al.*, 2002). To address the ability of Sro7 to interact with the IQ domain of Myo2 without affecting the length of the neck region of Myo2, we generated point mutations in each IQ domain. The strategy used to generate such mutants is shown in Figure 1C. Within each IQ motif, the three highly conserved charged amino acids important for recognition by light chains Mlc1 and CaM (Li and Sacks, 2003) were replaced by alanine. The six mutant forms and the wild-type form of the Myo2-IQ domain (782–925) were in vitro translated and tested for binding to purified ProtA-Sro7 on beads (Figure 1C). The results, shown in Figure 1C, demonstrated a pronounced effect for the IQ1 mutant and a smaller but statistically significant effect for the IQ5 mutant in binding assays with Sro7. We also examined the effect of double mutations in the IQ1 and IQ5 motifs of Myo2 (*myo2-iq1,5*) and found that this mutant showed similar defects as the single *myo2-iq1* mutant in the in vitro binding assay (Figure 1C).

In contrast, when the identical set of mutant proteins was examined in binding to recombinant glutathione *S*-transferase (GST)–Mlc1, a nonoverlapping set of binding perturbations was found. Mutations in IQ3 showed the strongest loss of binding, followed by smaller effects with mutations in IQ2 and IQ4. In addition, GST-Mlc1 showed strong binding to the in vitro–translated tandem IQ repeats from yeast Myo1, while Sro7 showed only very weak binding to the Myo1 IQ motifs (Figure 1C). Therefore each of Sro7 and Mlc1 appears to have distinct preferences for particular types of IQ repeats in this assay—suggesting a possible means for selectively disrupting this interaction in vivo.

To study the in vivo significance of the in vitro binding data, each of the *MYO2* single IQ mutants and the double IQ mutant (*myo2-iq1,5*) were transformed into yeast as the only source of Myo2 in the cell. Each of the IQ domain mutants described above was introduced into yeast by replacement of the *myo2-Δ6IQ* in a heterozygous diploid strain by homologous recombination (see *Materials and Methods*). Diploids were sporulated and subjected to tetrad analysis to identify haploids with the IQ mutations as the sole copy of *MYO2* in the cell. While the individual iq mutants showed little effect on growth under the conditions tested, the combination of the iq1

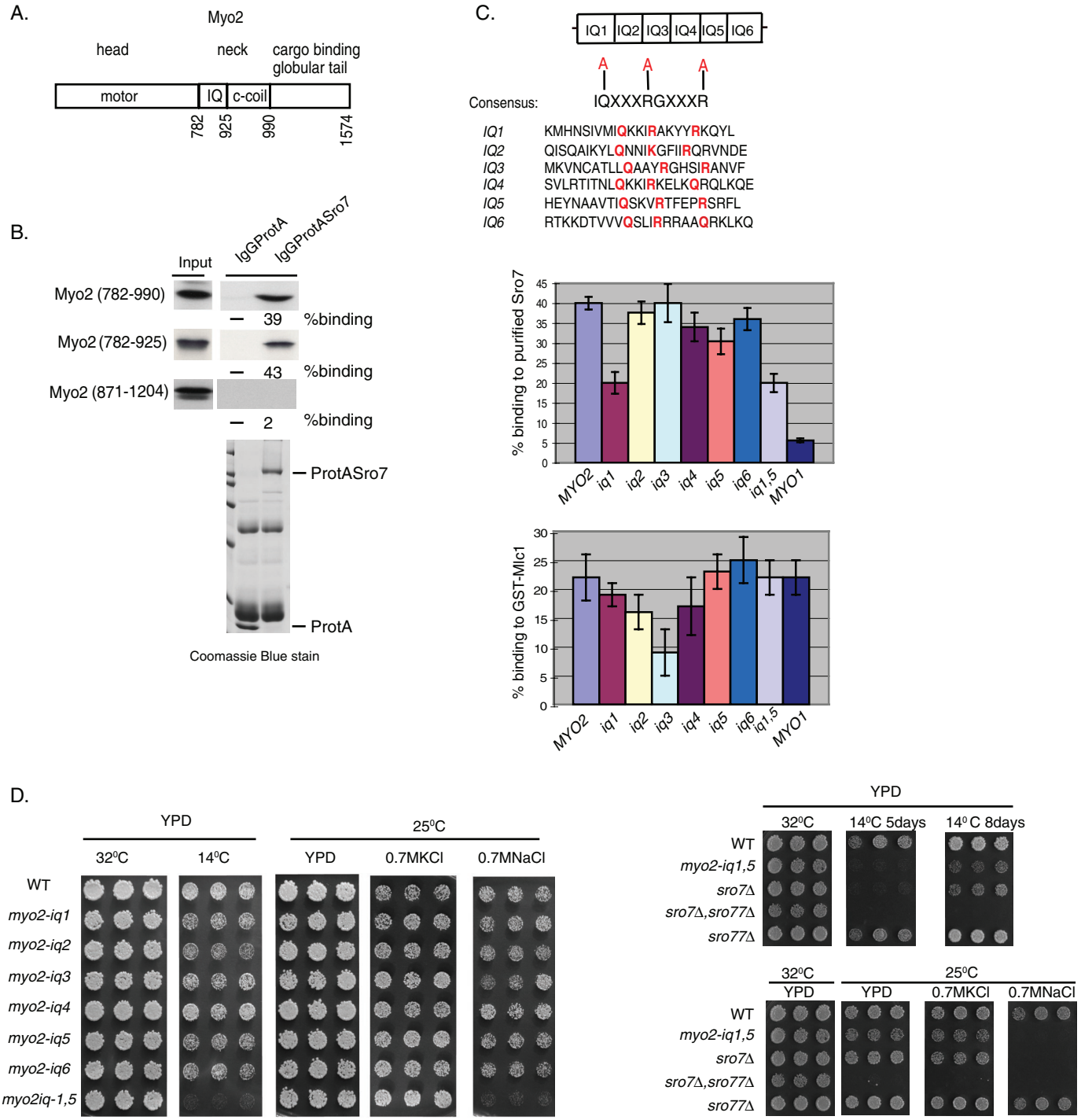

FIGURE 1: Identification of *myo2-iq1,5*, a novel myosin mutant that phenocopies a loss of Sro7 function. (A) Schematic representation of the type V motor, Myo2. (B) Minimum domain required for binding to Sro7. Radiolabeled fragments of the neck region of Myo2 were obtained by in vitro translation and bound to purified protASro7 on beads. (C) Strategy for generating point mutations in the IQ motif and effects of such mutations on binding to Sro7. Alanine substitutions made are shown in red. Charts show the results of binding assays between radiolabeled wild-type Myo2 (782–990) or Myo2 mutants (782–990) and protASro7 or control GST-Mlc1 on beads. Error bars represent the SD from three independent experiments. Binding of the IQ region of Myo1 (761–932) is shown on the extreme right of each chart as a comparison. (D) Three individual colonies of haploid yeast containing mutations in the IQ domain of Myo2 were picked into microtiter wells, transferred to YPD at the indicated temperatures and salt concentrations, and compared with haploid yeast containing mutations in *sro7*Δ, *sro77*Δ, and *sro7*Δ*; sro77*Δ.

and iq5 mutation (*myo2-iq1,5*) showed a dramatic loss of growth at low temperatures (Figure 1D)—a phenotype similar to that of *sro7*Δ, *sro77*Δ yeast in response to cold (Lehman *et al.*, 1999). The synthetic effect of the combination of the IQ1 and IQ5 mutations observed in vivo is more severe than that observed in vitro, perhaps reflecting functional redundancy for these sites in vivo. Moreover, the in vitro

binding data may not precisely reflect the in vivo situation due to the lack of competition from other IQ interacting proteins such as Mlc1. In addition to cold sensitivity, a second hallmark of loss of Sro7/77 function in yeast is sensitivity to high-sodium salts but not high-potassium salts (Larsson *et al.*, 1998). We therefore examined the effects of the iq mutants on yeast peptone dextrose (YPD) media with 0.7 M KCl and 0.7 M NaCl. The results, shown in Figure 1D, revealed that, like the *sro7*Δ mutant, the *myo2-iq1,5* mutant exhibits dramatic growth defects on YPD plates containing 0.7 M NaCl but not on 0.7M KCl. As with the cold sensitivity, none of the individual iq alleles showed any significant growth defect in high salt, suggesting that in vivo both IQ motifs function redundantly in their interaction with Sro7. Taken together these data suggest that the mutant form of Myo2, which demonstrates a specific defect in binding to Sro7 in vitro, exhibits phenotypes similar to those seen when Sro7 function is compromised in vivo. Therefore the phenotypes observed in the *myo2-iq1,5* mutant strongly suggest that Myo2 plays an important role in the regulation of Sro7 function in vivo.

The *myo2-iq1,5* mutant displays a cold-sensitive defect in post-Golgi secretion

Analysis of the growth properties of the *myo2-iq1,5* mutant in liquid culture demonstrated a dramatic growth defect at 25°C when compared with growth at 32°C (Figure 2A, Figure 1D). We have previously shown that loss of Sro7 function is accompanied by the accumulation of post-Golgi secretory vesicles and defects in secretion of invertase and Bgl2 (Lehman *et al.*, 1999; Hattendorf *et al.*, 2007). We therefore examined the secretory function of *myo2iq-1,5* strains grown at permissive temperature (32°C) or after an 8-h shift to the nonpermissive temperature (25°C). As a positive control we used a well-characterized secretory mutant, *sec4P-48*, which acts at the same stage of the pathway and shows growth and secretion defects in the same temperature range as *myo2-iq1,5* (Brennwald *et al.*, 1994). Results from the secretion assays (Figure 2B) showed that there was a clear defect in Bgl2 secretion and a small, but significant, effect on invertase secretion upon a shift to the restrictive temperature in the *myo2iq-1,5* strain. Moreover, the accumulation correlated with a dramatic increase in the penetrance and number of post-Golgi vesicles (80–100 nm in size) observed within the bud and the mother cell imaged by thin-section electron microscopy (Figure 2C). Quantitation of the penetrance of this effect demonstrated that the *myo2-iq1,5* mutant showed 56% of cells with greater than 10 vesicles at 25°C, while only 19% of the mutant cells exhibited greater than 10 vesicles at 32°C. As expected, none of the isogenic wild-type cells showed vesicle accumulation at either temperature (Supplemental Figure 1). Therefore, like the *sro7*Δ, *sro77*Δ mutant, the *myo2iq-1,5* mutant shows a cold-sensitive defect in growth and post-Golgi secretion.

Sro7 polarization is lost in the *myo2-iq1,5* mutant strain

To look for possible effects of the *myo2iq-1,5* mutant on the subcellular localization of Sro7, we generated a tagged form of Sro7 containing three tandem copies of green fluorescent protein (GFP) inserted at the N-terminus (Supplemental Figure 2) of the Sro7 coding sequence. Attempts to fuse GFP at the C-terminus of the protein resulted in loss of function (scored by complementation of the *sro7*Δ, *sro77*Δ mutant), as this region is essential (Hattendorf *et al.*, 2007). Three copies of GFP were required to detect Sro7 expressed behind its own promoter from a single-copy (*CEN*) plasmid. The GFP-tagged *SRO7* fully complemented both the cold sensitivity and salt sensitivity of the *sro7*Δ, *sro77*Δ strain, suggesting that the introduction of a GFP tag at the N-terminus of the protein did not affect function (Supplemental Figure 2). Western blot analysis of whole-cell extracts from cells containing the *GFP-SRO7* allele expressed a protein of the expected mobility that was present at levels just slightly above (2.5×) that of the endogenous Sro7 protein (Supplemental Figure 2). As shown in Figure 3A, GFP-Sro7 was concentrated in the bud of growing cells and at sites of division in cells undergoing cytokinesis.

To study whether polarized localization of Sro7 requires the interaction with the IQ domain of Myo2, wild-type and *myo2-iq1,5* mutant cells were transformed with GFP-Sro7 and examined by fluorescence microscopy. Overall polarity in the *myo2-iq1,5* mutant was monitored by comparing GFP-Sro7 polarization to that of GFP-Sec4 introduced under identical conditions into the mutant strain, as polarization of the Sec4 GTPase is known to be affected rapidly by a perturbation of Myo2-dependent vesicle transport (Pruyne *et al.*, 1998). GFP-Mlc1 was also transformed in both wild-type and mutant *myo2-iq1,5* cells to determine whether the specificity of the IQ1 and IQ5 mutations was through an effect on Sro7 and not by perturbing the polarization of the Myo2 myosin light chain, Mlc1. The results in Figure 3B show a remarkably specific effect of the *myo2-iq1,5* mutant on polarity of Sro7. GFP-Sec4 and GFP-Mlc1 fluorescence in the *myo2-iq1,5* mutant strain was comparable to the wild type. However, under these same conditions, GFP-Sro7 did not localize to sites of polarized growth and appeared diffuse in ~95% of the small budded cells analyzed. Coimmunoprecipitation experiments with *MYO2* or *myo2-iq1,5* strains demonstrated that while Sro7 could readily be detected in anti-Myo2 immunoprecipitations, we failed to see any detectable coimmunoprecipitation of Sro7 from *myo2-iq1,5* cells (Figure 3C). Taken together, these results indicate that mutations in the IQ region of Myo2 that disrupt Sro7 binding in vitro also disrupt the association in vivo and have a highly selective effect on the polarized localization of GFP-Sro7 without affecting the overall polarity of the cell. Moreover, these data suggest that the loss of Sro7 polarization in these cells may be responsible for the cold-sensitive secretory phenotypes observed in the *myo2iq-1,5* mutant strain (Figure 2, B and C).

Sro7 polarization appears to be the product of delivery on post-Golgi vesicles

Many components of the late secretory apparatus have a polarized staining pattern similar to that seen for Sro7—including the Sec4 GTPase, the Sec4 exchange factor Sec2, and components of the exocyst complex (Goud *et al.*, 1988; Walch-Solimena *et al.*, 1997; Boyd *et al.*, 2004). In each of these cases, the observed localization was found to be mediated by a Myo2-dependent polarized delivery of vesicles along actin cables. To address the possibility of the Myo2-dependent pathway for Sro7 polarization, we first examined the degree of colocalization between GFP-Sro7 and the vesicle marker red fluorescent protein (RFP)–Sec2 in strains coexpressing both markers. For these results we focused on fixed cells where discrete RFP-Sec2 particles (which in live cells are seen to move toward sites of growth) were clearly visible. The results, shown in Figure 4A, showed a high degree of colocalization (85%) of GFP-Sro7 with RFP-Sec2, supporting the possibility that Sro7 is associated with the Sec4/Sec2/Myo2 system of vesicle delivery. There is still, however, a significant fraction of Sec2-containing particles in which Sro7 is not detectable, as only 58% of the total RFP particles colocalized with the GFP particles. To determine whether the polarized staining of GFP-Sro7 was dependent on the Sec4/Sec2/Myo2 post-Golgi vesicles delivery system, we examined the fate of GFP-Sro7 in mutants in this delivery system. For example, polarized Sec4 delivery is known to be lost in *myo2-66* and *sec2-41* mutants, but it remains polarized in a *sec6-4* mutant, which is required for vesicle docking and not polarized delivery (Walch-Solimena *et al.*, 1997; Pruyne *et al.*, 1998). We

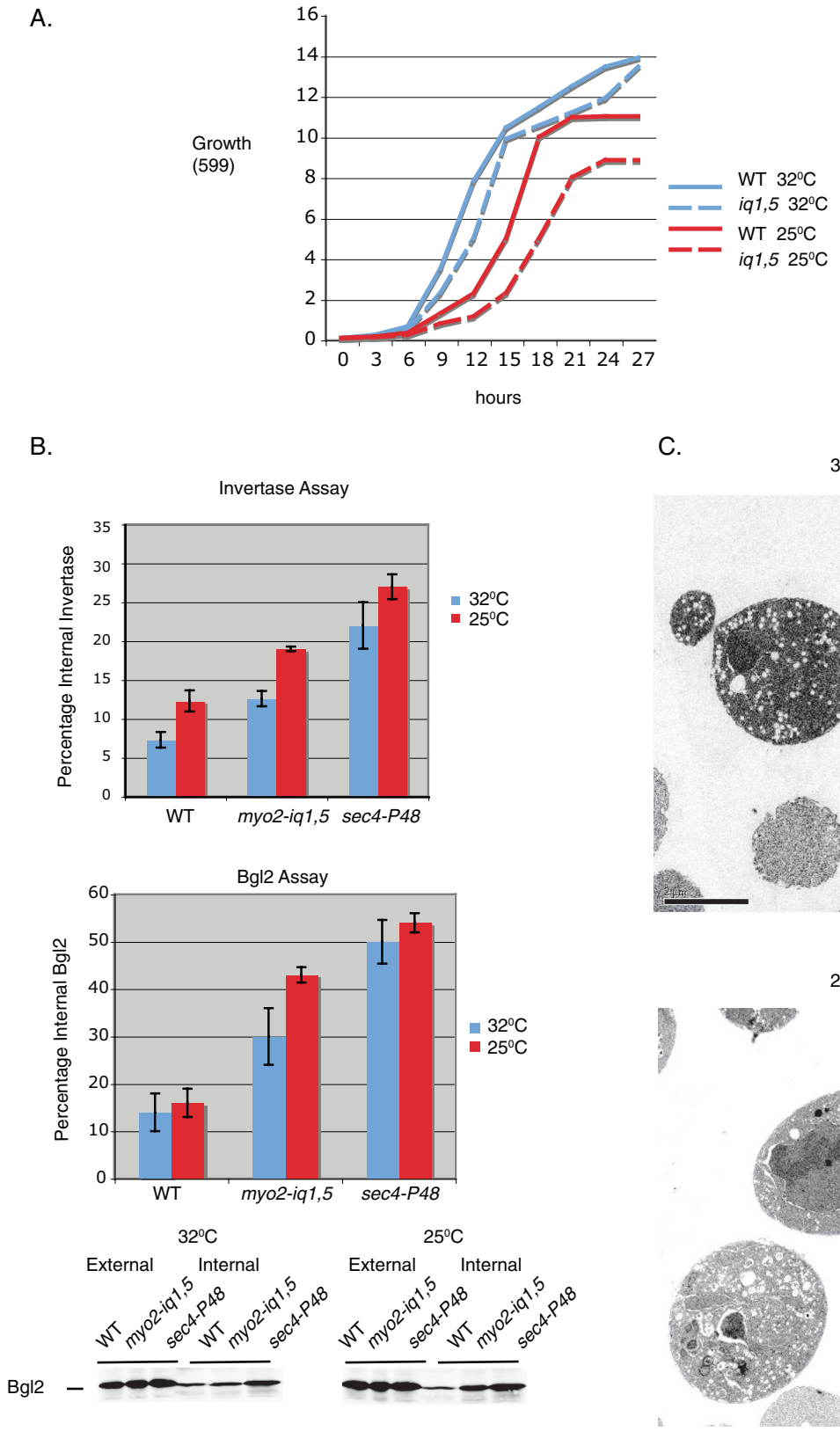

FIGURE 2: The *myo2-iq1,5* mutant shows a pronounced cold-sensitive secretory defect in post-Golgi transport. (A) Wild-type and the *myo2-iq1,5* mutant were grown at the permissive temperature of 32°C and then shifted to the restrictive temperature of 25°C. Growth at both temperatures was monitored at 3-h intervals in YPD media. (B) Graphs show results of invertase and Bgl2 assays conducted on wild-type, *myo2-iq1,5*, and the *sec4-P48* mutants after a shift to the restrictive temperature of 25°C for 8 h. Error bars represent the SD from three independent experiments. A representative blot of a Bgl2 assay is shown. (C) *myo2-iq1,5* cells grown under permissive conditions (32°C) or grown at 32°C and then shifted to restrictive conditions (25°C) for 8 h were fixed and processed for electron microscopy.

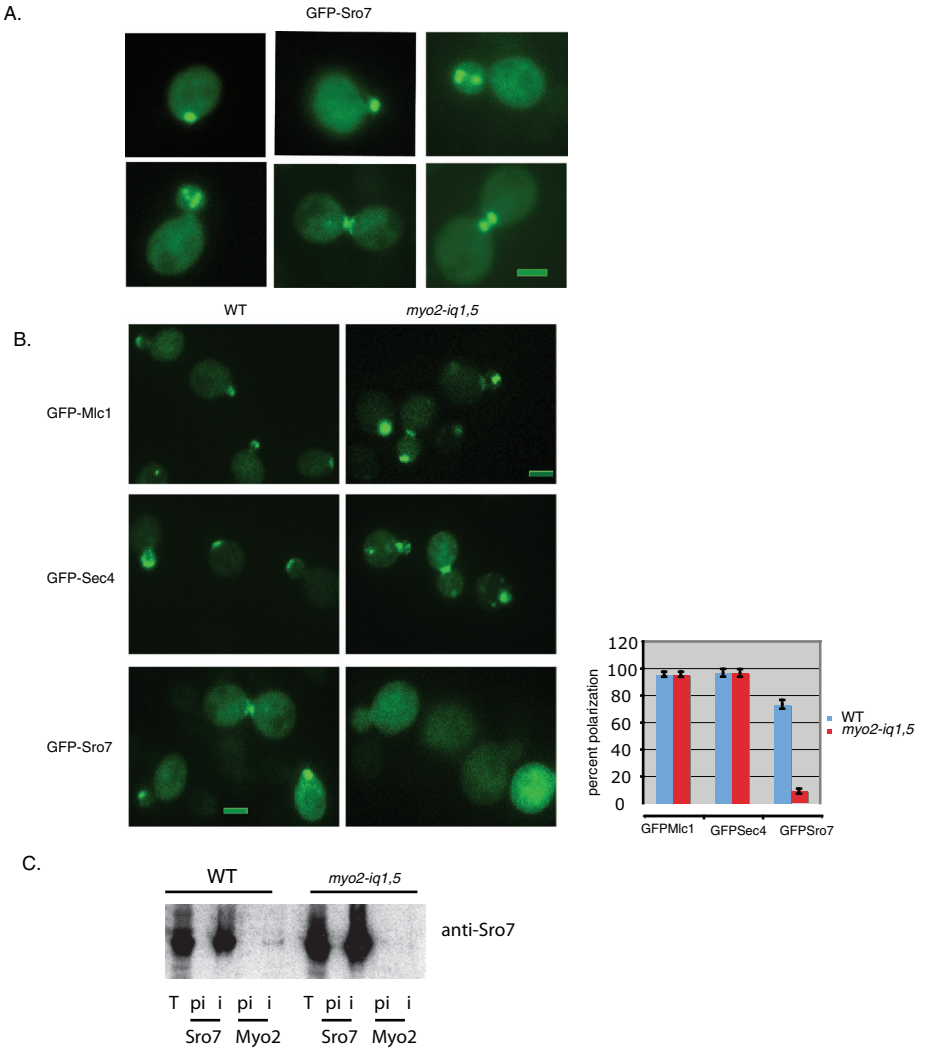

FIGURE 3: GFP-Sro7 polarization to sites of active growth is dramatically perturbed in the *myo2-iq1,5* mutant. (A) Wild-type strain expressing GFP-Sro7 (*CEN*) was grown in selective media to midlog at 25°C and then fixed and processed for fluorescence microscopy. Bar, 1 μm. (B) Wild-type and *myo2-iq1,5* strains expressing GFP-Sro7 (*CEN*), GFP-Sec4 (*CEN*), and GFP-Mlc1 (*CEN*) were grown in selective media at the permissive temperature (32°C) and then fixed and processed for fluorescence microscopy. Quantitation of polarized tagged proteins in wild-type and *myo2-iq1,5* mutant cells were obtained by scoring a minimum of 50 cells at emerging bud sites and bud tips. Bar, 1 μm. (C) Wild-type and *myo2-iq1,5* mutant cells were grown overnight at permissive temperature (32°C) and then shifted to 25°C for 8 h before being spheroplasted, lysed, and subjected to immunoprecipitation with affinity-purified preimmune (pi) and immune (i) anti-Sro7 and anti-Myo2 antibody. The lane marked T represents the input of wild-type and *myo2iq1,5* strains used.

therefore examined the effect of *sec6-4*, *myo2-66*, and *sec2-41* mutants on the localization of GFP-Sro7 following a shift to the restrictive temperature. The results, shown in Figure 4B, demonstrate that while GFP-Sro7 maintains its polarity in *sec6-4* and wild-type cells, polarity is drastically lost in the *myo2-66* and *sec2-41* mutant backgrounds. This result is identical to the effects of these mutants on Sec4 localization and suggests that Sro7 is brought to sites of polarized growth by delivery with post-Golgi vesicles.

Sro7 forms large clusters of post-Golgi vesicles in the *myo2-iq1,5* mutant when expressed from a moderate promoter

When overexpressed, Sro7 is able to rescue a number of mutants defective in the late secretory pathway, including *cdc42-6*, *rho3-V51*, *sec4-P48*, *sec3-2*, *sec8-9*, and *sec15-1* (Lehman *et al.*, 1999; Adamo *et al.*, 2001). To understand whether increasing the expression of Sro7 in the *myo2-iq1,5* strain would rescue the growth defect observed in this mutant, we transformed wild-type and the *myo2-iq1,5* strain with a plasmid that expressed Sro7 from a tetracycline-repressible promoter. This promoter is repressed in the presence of doxycycline, and in the absence of doxycycline it increases the level of Sro7 approximately five times over the level of endogenous Sro7. As expected, the presence of the tet-Sro7 plasmid strongly suppressed the temperature-sensitive growth defect of *sec15-1* strains grown in the absence of doxycycline but failed to suppress in the presence of doxycycline (Figure 5A). This plasmid did not affect growth in wild-type cells. To our surprise we found that the *myo2-iq1,5* mutant was not suppressed by Sro7 overexpression but rather demonstrated a strong doxycycline-dependent inhibition of growth that was most apparent at 25°C (Figure 5A).

To understand the dominant negative effect of Sro7 overexpression on *myo2-iq1,5* cells, we transformed these strains with a plasmid expressing GFP-Sec4 (*CEN*) and examined Sec4 localization by fluorescence microscopy. Like Sec2, GFP-Sec4 is an abundant marker for the vesicle delivery system in yeast (Pruyne *et al.*, 1998) and is found associated with sites of polarized growth. Following induction of Sro7, the distribution of GFP-Sec4 changed drastically and appeared as large "patches" in the cytoplasm (Figure 5B). When we examined these cells by thin-section electron microscopy, we found the appearance of large clusters of 80–100 nm vesicles (Figure 5C). Quantitation of the electron micrographs demonstrate that 92% of the *TET-SRO7/myo2-iq1,5* cells exhibited vesicle clusters, while only 7% of the *TET-SRO7/MYO2* cells and 12.5% of the *TET* empty vector/*myo2-iq1,5* cells exhibited vesicle clustering. No cells were observed with vesicle clusters in the empty vector control/*MYO2* combination. Therefore *myo2-iq1,5* cells appear to be specifically sensitive to moderate overexpression of Sro7 in the tet-repressible expression system. This sensitivity is seen as an effect on growth and vesicle patch formation, observed by both fluorescence and electron microscopy. This phenomenon is remarkably similar to the effect of overexpression of another well-characterized Sec4 effector protein, Sec15, suggesting that vesicle clustering may be a common feature of overregulation of Sec4 function in membrane tethering (Salminen and Novick, 1989).

Sro7 and Sec15 cause Sec4-dependent vesicle clustering when expressed under a strong promoter in wild-type cells

Previous work describing the vesicle clustering property of Sec15 overexpression made use of a strong inducible *GAL1/10* promoter.

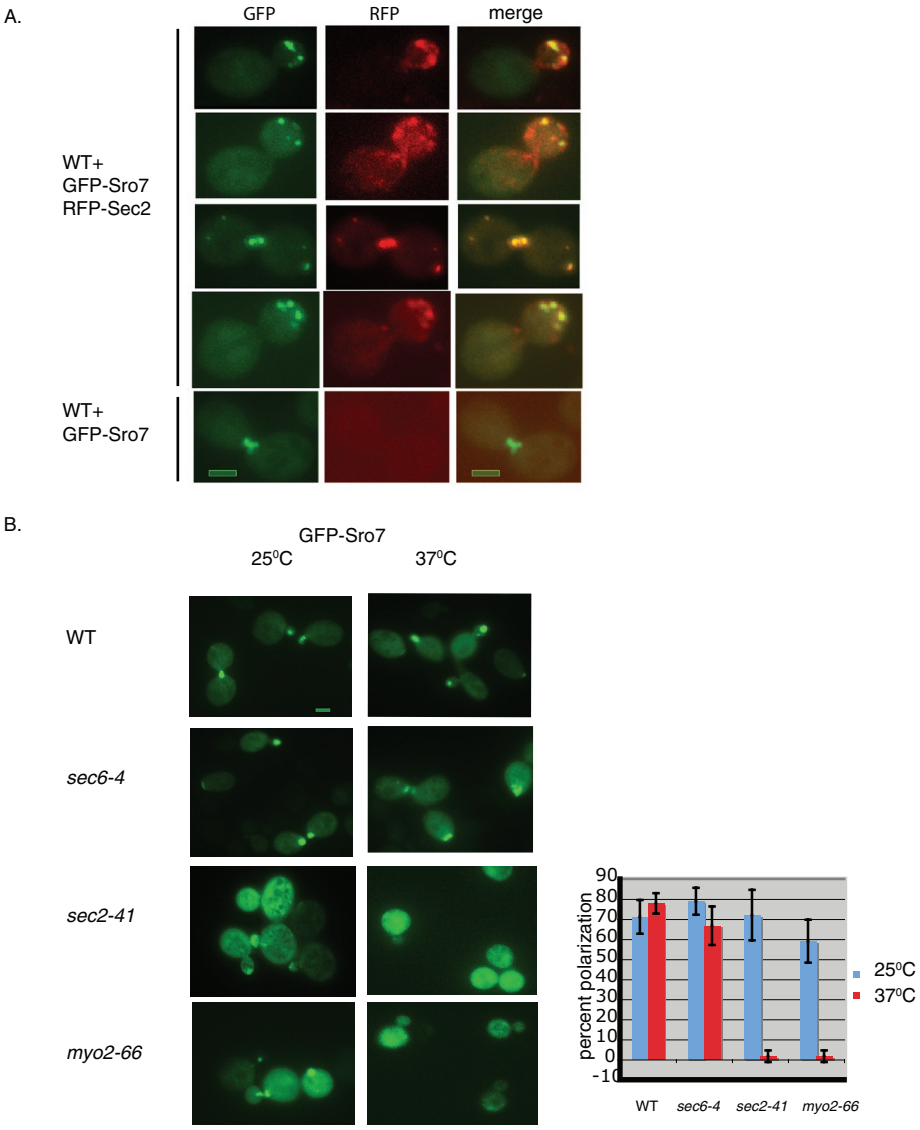

FIGURE 4: Sro7 polarization appears to be the product of delivery on post-Golgi vesicles. Cells expressing both GFP-Sro7 (*CEN*) and RFP-Sec2 (*CEN*) were grown in selective media overnight and then fixed and processed for fluorescence microscopy. The merged image of GFP-Sro7 and RFP-Sec2 fluorescence is shown on the right. Bar, 1 μm. (D) Wild-type, *sec6-4*, *sec2-41*, and *myo2-66* mutant strains containing GFP-Sro7 were grown in selective media to midlog at 25°C and then shifted to 37°C for 1 h before fixing and processing for fluorescence microscopy. Quantitation of GFP-Sro7 polarization was obtained by scoring a minimum of 50 cells for the presence of GFP-Sro7 at emerging bud sites and bud tips.

GAL-SEC15 showed a strong inhibition of growth in wild-type yeast but not in *sec4-8* or *sec2-41* mutants (Salminen and Novick, 1989), suggesting that a functional Rab (Sec4) is required in order to induce vesicle clustering and growth inhibition. To directly compare effects of the two Sec4 effector proteins on vesicle clustering, both open reading frames of Sro7 and Sec15 were put under the control of the strong galactose-inducible promoter and transformed into wild-type stains and various late *sec* mutant strains by integrative transformation. As seen previously, the *GAL-SEC15* transformants exhibited a severe inhibition of growth in wild-type and *sec9-4* strains when grown on galactose-containing media (Figure 6A). In contrast, no growth inhibition was observed in the *sec2-41* or *sec4-8* mutants, as previously reported (Salminen and Novick, 1989). Interestingly, we saw a strikingly similar pattern when *GAL-SRO7* was introduced into wild-type and the same set of secretory mutants: *sec9-4*, *sec2-41*, and *sec4-8* (Figure 6A). Quantitative Western blot analysis suggests that the level of overexpression of Sro7 is ~16 times over the endogenous level following a 10-h induction (Figure 6B)—similar to the levels of overexpression reported for *GAL-SEC15* (Salminen and Novick, 1989). The similar pattern of growth arrest for *GAL-SRO7* and *GAL-SEC15* suggests that the overexpression of these Rab effectors might result in a related effect on post-Golgi trafficking downstream of Sec4. We therefore examined the *GAL-SRO7*– and *GAL-SEC15*–induced cells by thin-section electron microscopy. As previously observed, the *GAL-SEC15* strain showed a highly penetrant (70%) phenotype, where large clusters of 80–100 nm vesicles were present that were not observed in control wild-type cells (Figure 6C). Interestingly, we observed a nearly identical, highly penetrant (76%) accumulation of clusters of 80–100 nm vesicles in response to *GAL-SRO7* expression (Figure 6C). The striking similarity of growth and vesicle clustering phenotypes observed for these two Sec4 effectors strongly suggests that they occur through a common Sec4-dependent mechanism.

To further characterize the clustering of post-Golgi vesicles induced by *GAL-SEC15* and *GAL-SRO7*, we analyzed vesicle cluster formation by immunofluorescence microscopy using monoclonal antibodies to the post-Golgi vesicle marker, Sec4, and polyclonal antibodies to either Sro7 or Sec15. As seen in Figure 7 (A and B), conditions that led to vesicle cluster formation by electron microscopy correlated with the formation of a large patch of Sec4 staining within the cell, which differed significantly from polarized Sec4 staining (i.e., bud tips) in cells with no Sro7 or Sec15 overexpression. Consistent with the notion that the formation of the Sec4 patch is tightly linked to the growth arrest seen in Figure 6A, Sec4 patches were not observed in the *sec4-8* or *sec2-41* mutants, suggesting that activated GTP-bound Sec4 is required for *GAL-SEC15* and *GAL-SRO7* to induce vesicle clusters in the cell. As seen previously (Salminen and Novick, 1989), overexpression of Sec15 results in pronounced accumulation of Sec15 staining by immunofluorescence that colocalizes precisely with the Sec4 patches that form in these cells (Figure 7A). Likewise we find that overexpression of Sro7 results in a pronounced accumulation of Sro7 staining in patches that colocalize precisely with Sec4 (Figure 7B). Therefore both Sec4 effectors appear to be physically associated with the vesicle clusters that they induce.

The N-terminal 13 amino acids of Sro7 are required for Myo2 binding and Sro7 polarization

As described above, *myo2-iq1,5* mutants show increased sensitivity to Sro7 such that even moderate overexpression from a

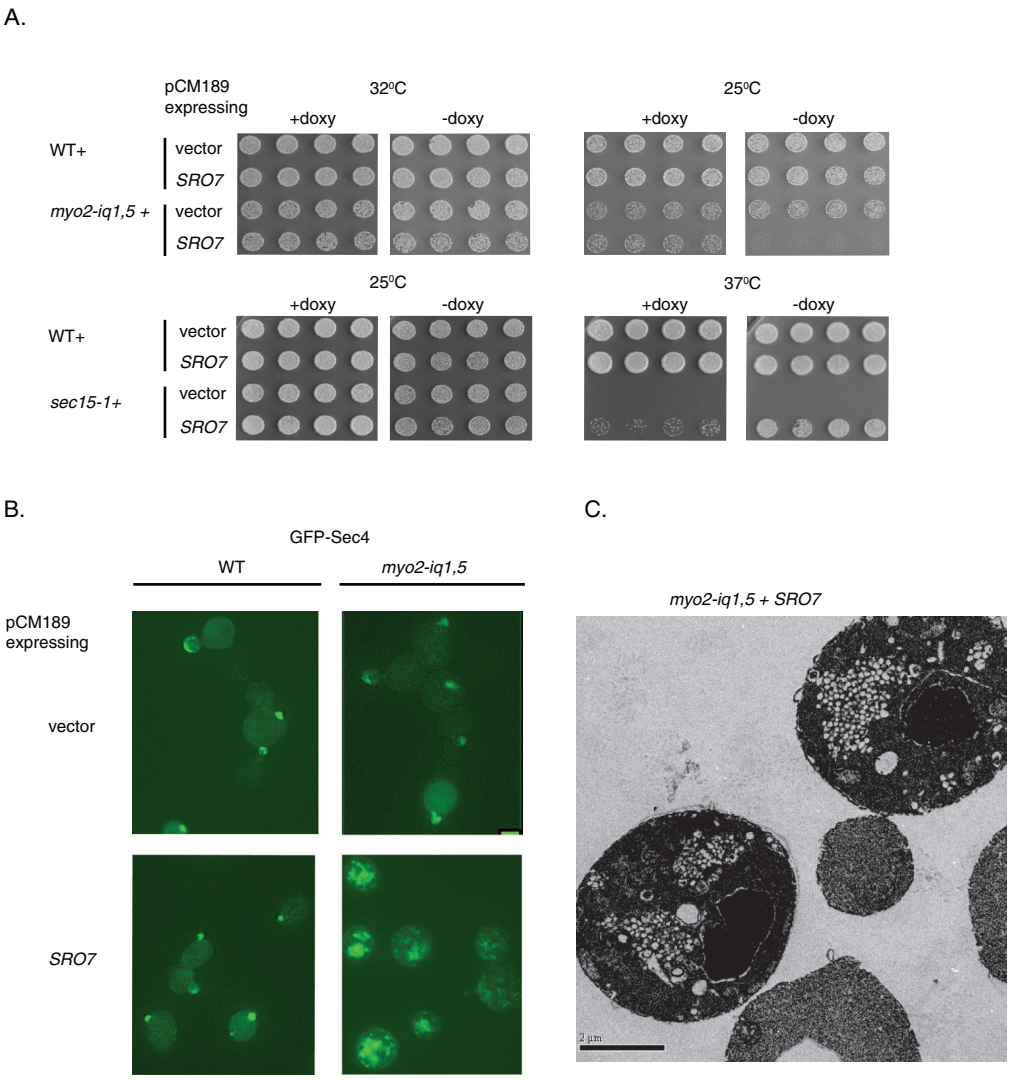

FIGURE 5: Sro7 forms large clusters of post-Golgi vesicles when expressed in the *myo2iq-1,5* mutant under a moderate promoter. (A) Wild-type, *myo2-iq1,5*, and *sec15-1* mutant cells were transformed with a plasmid expressing Sro7 behind a tetracycline-repressible promoter (*CEN*) or vector only. Four independent transformants were picked into microtiter wells and transferred to YPD in the presence or absence of doxycycline. (B) Wild-type and *myo2-iq1,5* mutant cells containing a Sro7 behind a tetracycline-repressible promoter (*CEN*) were transformed with *GFP-SEC4* (*CEN*). Cells were grown in selective media in the presence of doxycycline and then shifted to media lacking doxycycline to induce Sro7 expression for 8 h at 25°C. Cells were then fixed and processed for fluorescence microscopy (bar, 1 μm) and (C) electron microscopy.

tet-inducible promoter results in vesicle clustering and a pronounced inhibition of growth. This suggests a simple model in which the interaction between Myo2 with Sro7 helps to negatively regulate Sec4-dependent vesicle tethering. To further examine this model, we sought to identify the site of interaction on Sro7 that binds the IQ domains of Myo2. Previous work using chimeric swaps between Sro7 and mammalian Lgl (Gangar *et al.*, 2005) have demonstrated that neither the two WD propeller motifs nor the C-terminal domain of Sro7 is required for this interaction. Because these constructs contain the N-terminal 45 residues of Sro7 (Gangar *et al.*, 2005), we examined whether this region might contain the binding site for Myo2. Within this region, only the extreme N-terminus (4–18 in Sro7) shows conservation with Sro77 and other related ascomycetes members (Figure 8A). We therefore examined the binding of in vitro–translated Sro7, with large or small deletions in the N-terminus, to recombinant GST-Myo2IQ (782–990). As a positive control, a recombinant full-length form of the t-SNARE protein, Sec9, was used. Figure 8B shows that all of the mutant forms of Sro7 bound well to the t-SNARE, Sec9, as predicted by previous work (Hattendorf *et al.*, 2007). In contrast, while full-length Sro7 binds well to GST-Myo2IQ, both the large (Sro7-Δ[3–51]) and small (Sro7-Δ[4–18]) N-terminal deletions of Sro7 resulted in significant loss of interaction with GST-Myo2IQ. Therefore the conserved region within the extreme N-terminus of Sro7 appears to be required for binding to Myo2.

Because the data presented above suggest that the interaction of Sro7 with Myo2 is critical for the ability of GFP-Sro7 to be delivered to sites of polarized growth, we examined the effect of deleting this putative binding site on the polarization of GFP-Sro7. The result of this experiment, shown in Figure 8C, demonstrated that while the wild-type GFP-Sro7 protein is highly polarized, the N-terminal deletion mutant GFP–Sro7-Δ(4–18) showed diffuse cytoplasmic fluorescence and a loss of polarized localization at the bud tip. Consistent with the N-terminus of Sro7 being critical for the physical association between Myo2 and Sro7, when we examine the ability of wild-type and Sro7-Δ(3–51) proteins to coimmunoprecipitate with Myo2, we find that the mutant protein cannot detectably associate (Figure 8D). Taken together with the in vitro binding data, this experiment strongly supports the notion that the extreme N-terminus of Sro7 is required for its interaction with Myo2. Moreover, the similarity of this phenotype to that seen for wild-type GFP-Sro7 in the *myo2-iq1,5* mutant demonstrates the importance of the interaction with Myo2 for polarization of Sro7.

A predicted consequence of generating a form of Sro7 with reduced ability to interact with Myo2 is that it may result in a protein that would behave similarly to that of wild-type Sro7 in a *myo2-iq1,5* mutant background, where even moderate overexpression results in severe growth inhibition and vesicle clustering. Therefore we introduced the N-terminal mutant forms of Sro7 in the tet-repressible expression system and examined their effect when expressed in wild-type and several exocyst mutant backgrounds (*sec15-1*, *sec8-9*, and *exo70-113*). The results shown in Figure 8E demonstrate that, while dominant effects on growth were not apparent in wild-type cells, severe dominant effects on growth were apparent in response to the N-terminal deletion in three exocyst mutant strain backgrounds.

All dominant growth effects were lost in the presence of doxycycline, and no dominant effects on growth were observed for wild-type Sro7 expressed in any of these strains. The lack of a dominant effect for the N-terminal deletion mutants on wild-type cells might be a consequence of having a fully functional exocyst complex in these strains. Taken together it is apparent that loss of the site of Myo2 interaction within Sro7 generates a form of the protein that phenocopies many of the effects of the loss of the Sro7:Myo2 interaction in the *myo2-iq1,5* mutant. Importantly, the lethality induced by the N-terminal truncations of Sro7 in the exocyst mutant backgrounds (*sec15-1* and *exo70-113*) correlates strongly with the appearance of Sec4-positive clusters in these cells, which are likely to represent clusters of post-Golgi vesicles (Figure 8F). This strongly supports the model that loss of Myo2 binding leads to an up-regulation of Sro7 function, leading in turn to the membrane (vesicle) clustering phenotypes observed here.

Because Myo2 and Sec4 appear to function in opposite directions with regard to Sro7 function in vesicle clustering, we hypothesized that binding of Myo2 to Sro7 may directly or indirectly effect binding of Sro7 to Sec4-GTP. To examine this notion directly, we tested the effect of adding the purified Myo2 neck region (containing the six IQ repeats and the coiled-coil domain) on the binding of purified full-length Sro7 to Sec4-GTP in an in vitro binding assay (Grosshans *et al*., 2006). As a control we used the Myo2 neck region containing the IQ1 and IQ5 alanine point mutants described above. As we previously observed (Grosshans *et al*., 2006), we find the binding of Sro7 to Sec4 is highly dependent on the GTP-bound conformation of Sec4, as we see greater than fivefold stimulation in binding to GTPγS-bound Sec4 compared with guanosine 5′-diphosphate (GDP)–bound Sec4 (Figure 9). When we add 4 μM Myo2 neck region to the binding reaction, we see a 50% inhibition in the binding of Sro7 to Sec4-GTP. In contrast, no significant inhibition of binding was observed when 4 μM Myo2-IQ1,5 mutant protein was added to the binding assay. Therefore Myo2 not only antagonizes Sec4-Sro7 activity genetically but also antagonizes the physical interaction between Sro7 and Sec4 biochemically. This suggests a simple model (shown in Figure 9B) for the temporal and spatial regulation of Sro7 activity by Myo2, in which following its initial recruitment to the vesicle surface by Myo2, Sro7 would be maintained in an inactive form inaccessible for activation by the Rab GTPase, Sec4. Once arriving at the appropriate docking site, Myo2 would be displaced from Sro7 (by an as yet unknown mechanism—perhaps simply by high concentration of GTP-Sec4), and Sec4-GTP binding and activation of Sro7 would proceed—allowing docking and subsequent SNARE assembly and fusion to occur.

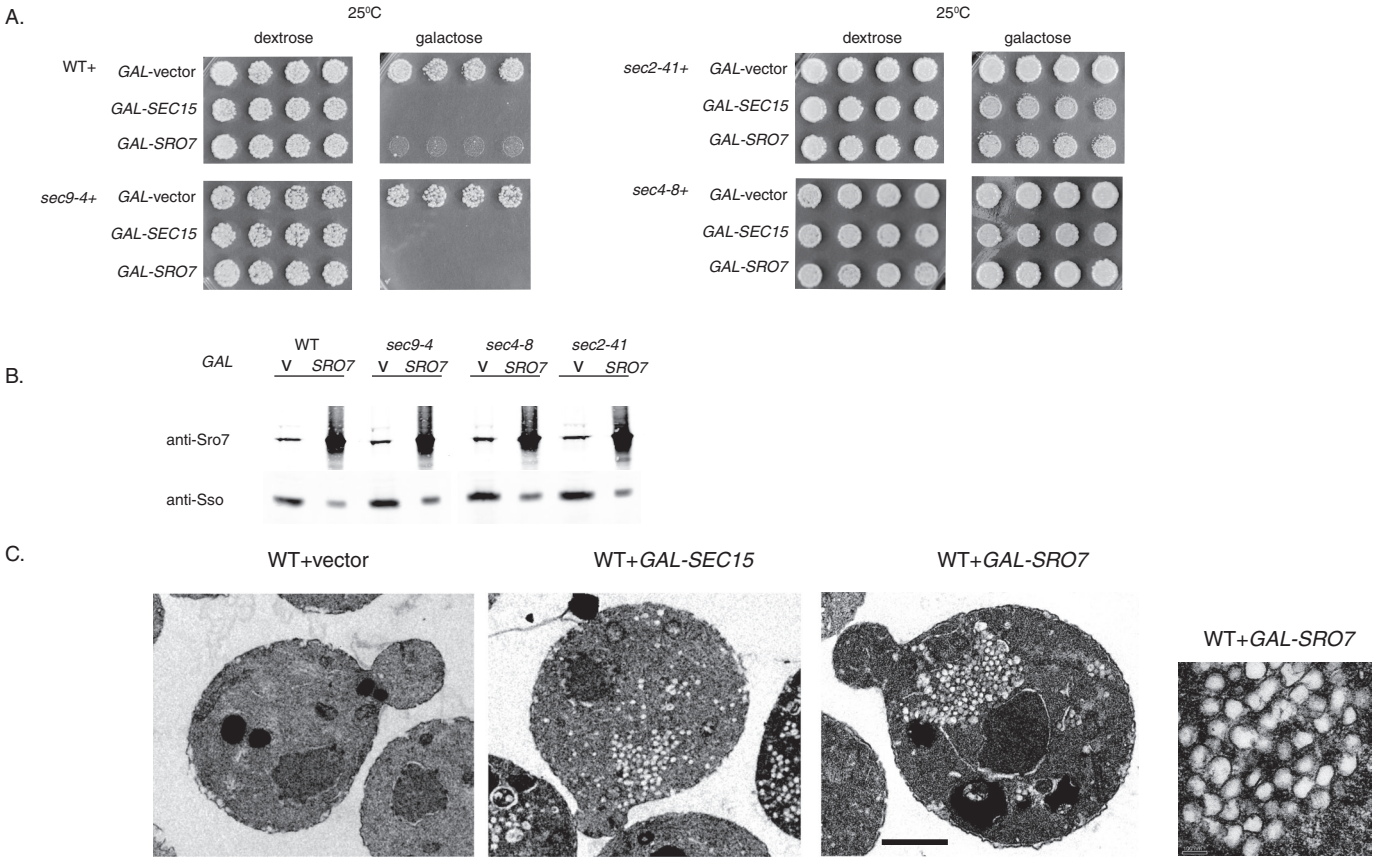

FIGURE 6: Sec15 and Sro7 drive formation of clusters of post-Golgi vesicles in wild-type cells when expressed from a strong promoter. (A) Vesicle clustering is Rab dependent and Sec9 t-SNARE independent. Wild-type, *sec4-8*, *sec2-41*, and *sec9-4* mutant strains were transformed with *GAL-SRO7* (Yip) or *GAL-SEC15* (Yip). Four individual colonies were picked into microtiter wells and then transferred onto YP plates containing dextrose or galactose. (B) Glass bead lysis and Western blot analyses was conducted to compare expression levels of Sro7 using anti-Sro7 and anti-Sso (control) rabbit polyclonal antibodies. (C) Wild-type strains expressing Sec15 or Sro7 from the galactose-inducible promoter (YIP) were grown in raffinose and then induced in galactose for 10 h at 25°C before fixing and processing for electron microscopy. Bar 1 μm. A high magnification is shown as an inset on the extreme right side of the figure.

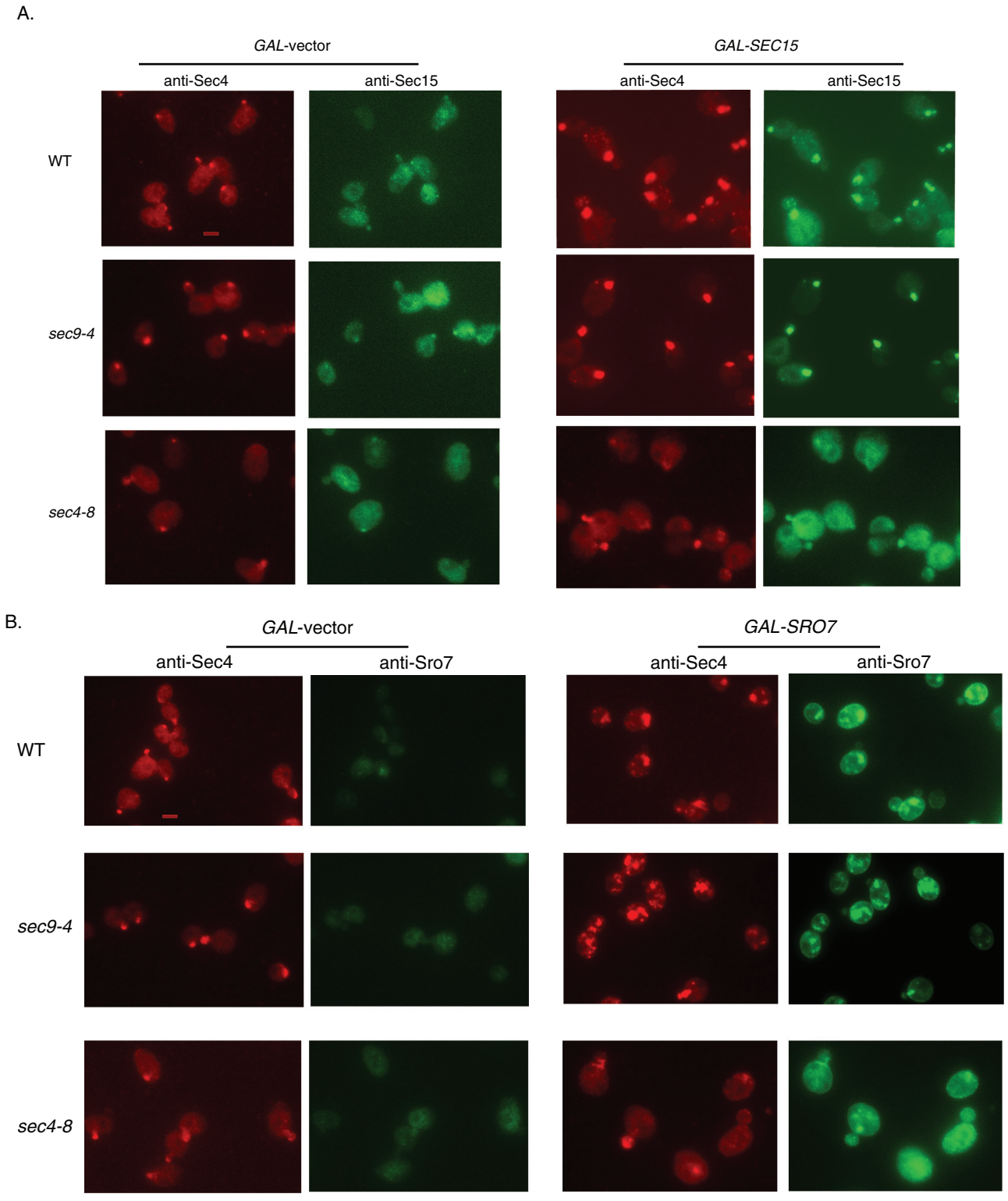

FIGURE 7: Overexpression of Sec15 or Sro7 correlates with the appearance of a bright patch of Sec4 in the cell. Wild-type, *sec9-4*, and *sec4-8* strains transformed with (A) *GAL-SEC15* (YIP) or (B) *GAL-SRO7* (YIP) were grown in raffinose and then induced with galactose for 10 h at 25°C. Cells were then fixed for immunofluorescence microscopy and analyzed with monoclonal anti–mouse Sec4 antibodies and polyclonal anti–rabbit Sec15 or Sro7 antibodies. Bar 1 μm.

DISCUSSION

In this article we characterize the cell biological, biochemical, and genetic significance of the interaction between the type V myosin Myo2 and the yeast lethal giant larvae homologue Sro7. Our data suggest that this interaction plays both positive and negative regulatory roles in modulating Sro7 function in polarized exocytosis. Alleles of *MYO2* encoding point mutations that selectively disrupt the interaction with Sro7 show specific defects in polarization of

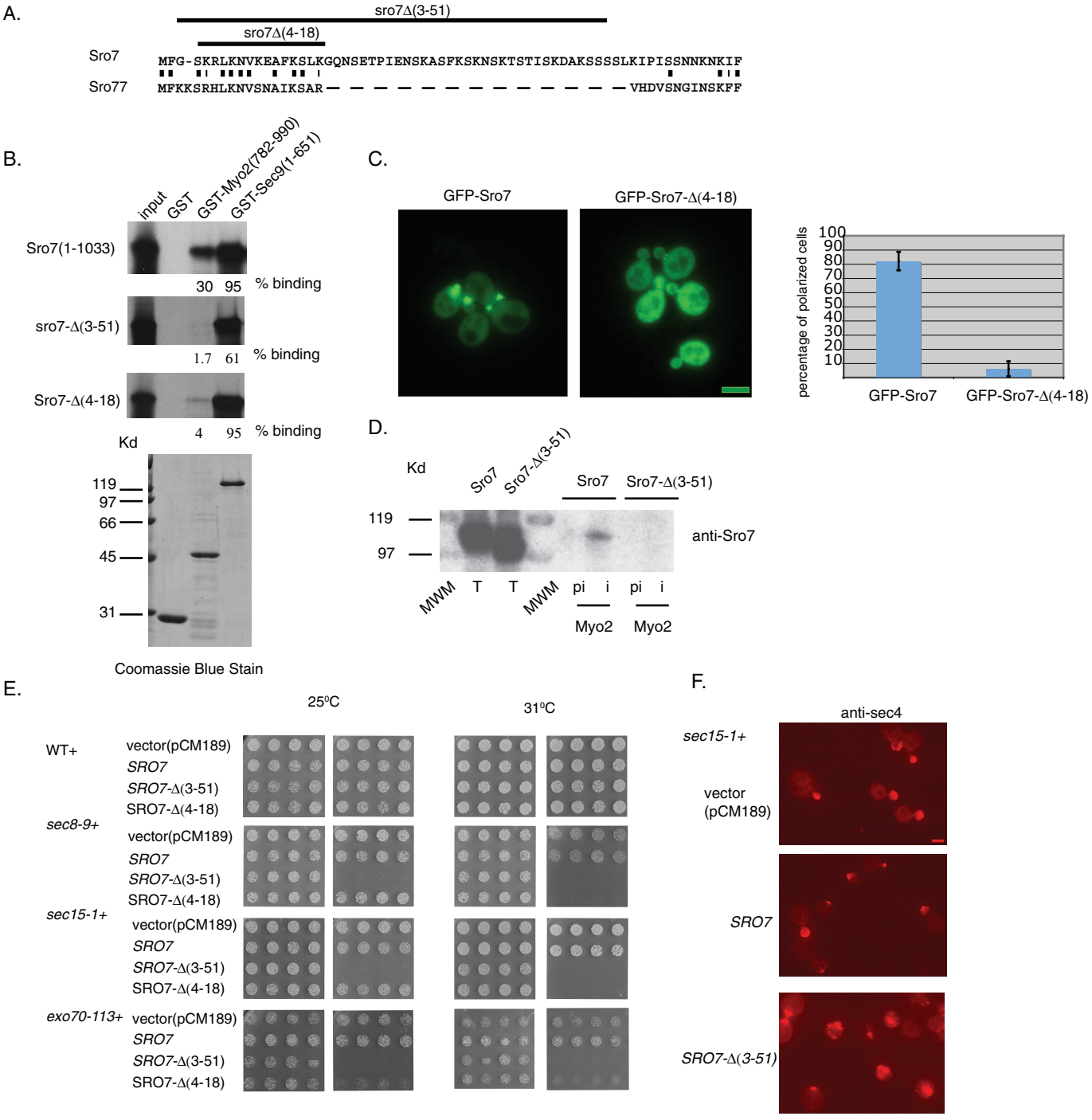

FIGURE 8: The N-terminal domain of Sro7 is required for the interaction with Myo2. (A) Alignment of the N-terminal region of Sro7 and Sro77 Lgl family members. (B) Deletion of the N-terminal domain of Sro7 affects binding to Myo2. Binding of radiolabeled, in vitro–translated full-length and N-terminal truncations of Sro7 to GST-Myo2IQ and GST-Sec9 on beads. (C) Wild-type cells expressing GFP-Sro7 (*CEN*) or GFP–Sro7-Δ(4–18) (*CEN*) were grown to midlog in selective media and then observed by fluorescence microscopy. Quantitation was obtained by scoring >50 cells for the presence of GFP fluorescence at emerging bud sites and bud tips. Bar 1 μm. (D) Wild-type cells expressing Sro7 or Sro7-Δ(3–51) behind a tetracycline-repressible promoter (CEN) were spheroplasted, lysed, and subjected to immunoprecipitation with affinity-purified preimmune and anti-Myo2 antibody. (E) Wild type, *sec15-1*, *sec8-9*, and *exo70-113* were transformed with a plasmid expressing Sro7, Sro7-Δ(3–51), or Sro7-Δ(4–18) behind a tetracycline-repressible promoter (*CEN*) or vector only. Four independent transformants were picked into microtiter wells and transferred to selective media in the presence or absence of doxycycline at different temperatures. (F) *sec15-1* mutant cells transformed with a plasmid expressing Sro7, Sro7-Δ(3–51), or vector only were grown at 25°C in the presence of doxycycline and then shifted to media without doxycycline for 8 h before fixing and processing for immunofluorescence with monoclonal anti-Sec4 antibody. Scale 1 μm.

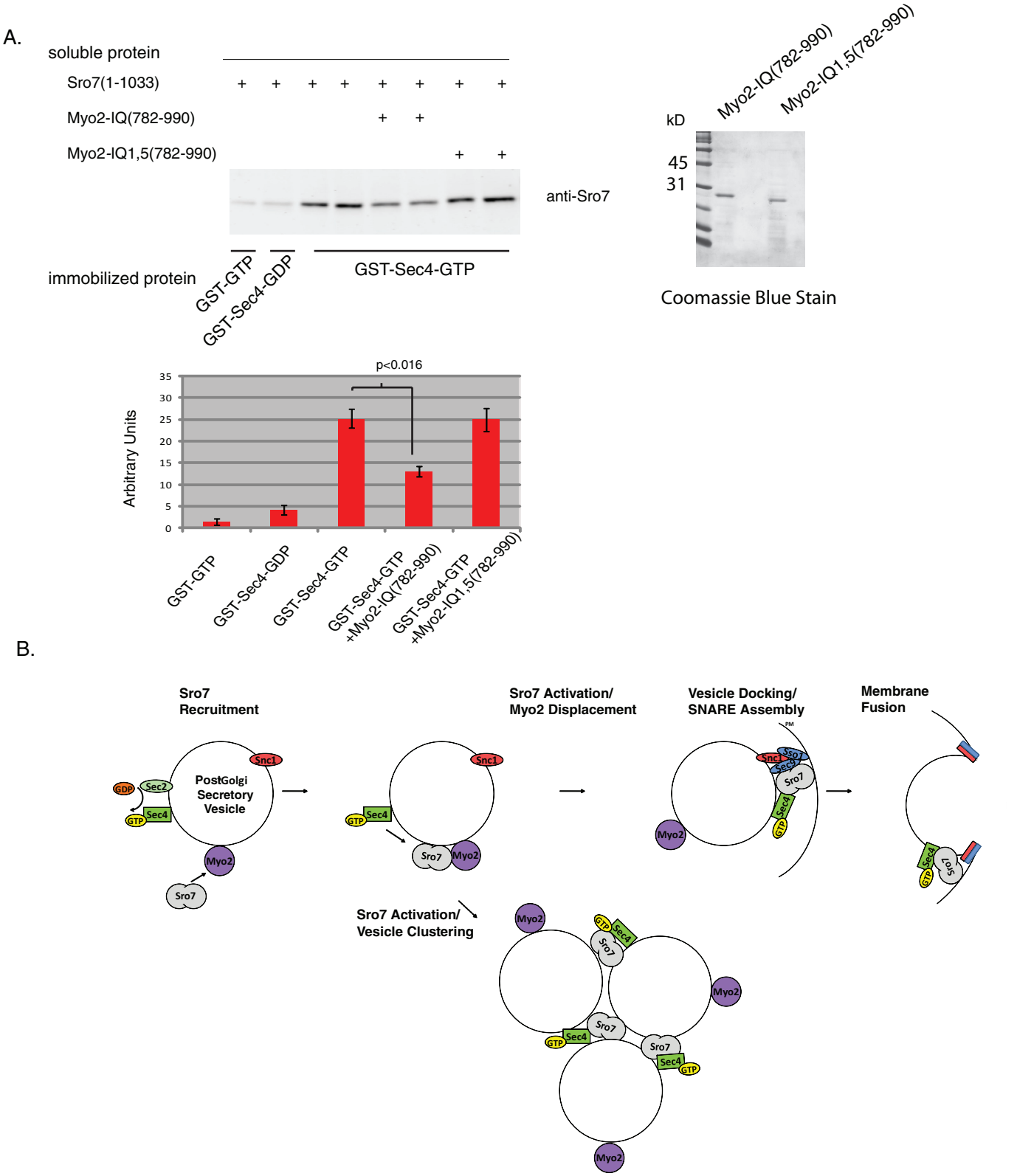

FIGURE 9: (A) The neck region containing the IQ motif of Myo2 is inhibitory to Sro7 binding to GTP bound Sec4. In vitro binding assays were conducted with GDP- or GTPγS-loaded Sec4 immobilized on glutathione Sepharose beads, soluble Sro7 (1 μM) and soluble wild-type IQ region of Myo2 (4 μM), or mutant Myo2IQ1,5 (4 μM). Graph shows results from four independent experiments, and SD and a Student's *t* test showed a p value < 0.016. (B) Model for the proposed function of Myo2 in Sro7 regulation of post-Golgi vesicle docking and fusion or in vesicle clustering.

GFP-Sro7 and show growth defects that are strikingly similar to those observed in *sro7*Δ, *sro77*Δ null mutants. These phenotypes are consistent with the notion that loss of Sro7 interaction with Myo2 results in cells that are unable to properly polarize Sro7, thus resulting in cold-sensitive and salt-sensitive growth and secretion defects similar to those observed with loss of Sro7/77 function. These results

strongly suggest that Myo2 has a positive role in promoting the polarity and overall function of Sro7 in exocytosis by aiding in the delivery of Sro7 to sites of active growth. A negative regulatory role of Myo2 on Sro7 became clear when we tried to determine whether moderate overexpression of Sro7 could suppress the growth defects associated with the *myo2-iq1,5* mutant. Previous work demonstrated that Sro7 overexpression was capable of suppressing a number of late-acting *sec* genes (Lehman *et al.*, 1999; Zhang *et al.*, 2005; Grosshans *et al.*, 2006). However, rather than suppressing the cold-sensitive and salt-sensitive growth defects associated with the *myo2-iq1,5* mutant, even moderate overexpression of Sro7 (using the tetracycline-repressible promoter) exhibited severe growth defects in the *myo2-iq1,5* mutant. This hypersensitivity to moderate Sro7 overexpression was not observed in wild-type cells and was in contrast to the ability of this same tet-repressible Sro7 construct to strongly suppress several late-acting *sec* mutants.

Interestingly, we found that the negative effect of Sro7 overexpression on growth correlated precisely with the appearance of post-Golgi vesicle "clusters" using both fluorescence and electron microscopy. Additional evidence for this negative mode of regulation appeared when we examined mutant forms of Sro7 that were defective in binding to Myo2. We found that moderate overexpression of Sro7 mutants defective in Myo2 binding induced dominant negative growth defects when expressed in several late-acting secretory mutants. These growth defects were also associated with the formation of vesicle clusters, suggesting that this is a common readout when Sro7 function is increased in the absence of Myo2 regulation.

The post-Golgi vesicle clustering phenotype we observed with increasing Sro7 function and/or loss of negative regulation by Myo2 has features that suggest the clustering phenomenon may be functionally related to post-Golgi vesicle tethering that normally occurs at the plasma membrane. First, the clustering phenomena—like many vesicle-tethering reactions examined in vitro (Pfeffer, 1999)—requires both a fully functional Rab GTPase (Sec4) and Rab exchange factor (Sec2) but occurs independent of t-SNARE function (Sec9). Second, overexpression of Rab effectors in other stages of membrane trafficking causes membrane clustering and thus may be a common effect of unregulated activation of the tethering machinery (Markgraf *et al.*, 2009; Yamamoto *et al.*, 2010). Third, the similarity of the phenotype of Sro7 overexpression with that of the Sec4 effector, Sec15 (which also clusters vesicles in a Sec4/Sec2-dependent but Sec9-independent manner), suggests that Rab effectors may generally help to promote membrane-to-membrane interaction when engaged by the GTP-bound Rab but that the specificity of this reaction is aided by other regulatory reactions that may keep it "off."

In fact, in a side-by-side comparison, we found that both Rab effectors, Sro7 and Sec15, behave virtually identically when placed behind the strong regulatable *GAL* promoter in wild-type cells. This supports the view that these two effectors work on parallel pathways at the same stage of vesicle transport to ensure proper tethering to the target membrane. The notion that multiple Rab effectors may play a synergistic role in promoting membrane tethering and fusion has recently been described and proposed as a mechanism for ensuring the specificity and efficiency of the process (Ohya *et al.*, 2009).

Previous studies on Sec4 have demonstrated a requirement for its exchange factor Sec2 in the Myo2-dependent delivery of vesicles to sites of polarized growth. This suggests the existence of an effector pathway for Sec4 that communicates information about the nucleotide state of the Rab onto the Myo2 motor. While it is possible that Sro7 might have such a role, we believe this is unlikely. This stems from the fact that we find that both the *myo2-iq1,5* mutant (Figure 3) and the *sro7Δ/sro77Δ* mutant (Gangar *et al.*, 2005) show normal polarization of Sec4 at sites of polarized growth—a phenotype that is known to be highly sensitive to Myo2-dependent vesicle delivery (Walch-Solimena *et al.*, 1997).

Previous work on Sro7 has characterized its role as an important regulator of SNARE complex assembly at sites of polarized growth at the plasma membrane. These results, however, highlight a novel role for Sro7 as a Rab-dependent tethering factor that acts in parallel to the exocyst complex. The data presented in this article suggest that, during polarized growth, Rab effector function must be tightly regulated and kept inactive until the vesicle is at the appropriate site on the correct target membrane. The type V myosin Myo2 may play such a role in the temporal and spatial regulation of Sro7 function. In such a model (Figure 9), Myo2 would help to recruit Sro7 to the surface of post-Golgi vesicles, but Sro7 would remain in a form that is inactive in promoting membrane tethering. On arrival to the target membrane, the inhibitory action would be relieved by displacement of Myo2 from Sro7, allowing Sec4- and Sro7-dependent tethering to the plasma membrane to occur. Displacement of Myo2 from Sro7 could occur through a number of possible triggering events. For example, interaction of Sro7 with the t-SNARE Sec9, the exocyst subunit Exo84, or both could represent displacement factors. Displacement activity could function through factors binding to a site on Sro7 that overlaps with that of Myo2, or through binding to a different site on Sro7 that induces a conformational change, preventing the N-terminus of Sro7 from being available for Myo2 binding. If the displacement factors were localized at higher concentrations to sites of polarized growth, such a mechanism may represent an important means of increasing the temporal and spatial specificity of vesicle-tethering reactions. Such a mechanism would aid not only in preventing vesicle:vesicle clustering but also in ensuring that tethering was unlikely to occur at inappropriate membranes.

Previous studies have demonstrated strong genetic interactions between Lgl homologues and both type II and type V myosins in flies and yeast (Kagami *et al.*, 1998; Peng *et al.*, 2000). In fly neuroblasts, Lgl and type II myosins appear to act antagonistically to each other in promoting polarized localization of cell fate determinants (Peng *et al.*, 2000). Likewise, antagonistic genetic interactions were observed between yeast Sro7 and type II myosin during cytokinesis (Kagami *et al.*, 1998). Therefore the negative regulatory role we observe here for Myo2 on Sro7 may utilize a conserved mechanism by which myosin motor proteins regulate Lgl family protein function in promoting cell polarity. In this way the regulatory interactions described in this work may be part of an ancestral mechanism for regulation of eukaryotic cell polarity through localized regulation of Lgl function. Further analysis of myosin-Lgl in other systems may be necessary to determine whether this is the case.

MATERIALS AND METHODS

Media and reagents

Strains were grown in either YP medium (1% bacto-yeast extract and 2% bacto-peptone; Difco, Sparks, MD), S minimal media (0.67 yeast nitrogen base; Difco, Sparks, MD), or dropout media lacking the appropriate amino acid (0.67 yeast nitrogen base with amino acid supplement; US Biological, Swampscott, MA) with 2% glucose. Strains for galactose inductions were grown in 3% raffinose and induced with 1% galactose (US Biological, Swampscott, MA). Nourseothricin sulphate was obtained from Sigma-Aldrich, St. Louis, MO. G418 sulphate was obtained from US Biological. Doxycycline hyclate was obtained from Sigma Aldrich, St. Louis, MO. Zymolyse 100T was obtained from Seikagaku America, Falmouth, MA. GTPγS was from

Roche Diagnostics, Indianapolis, IN. GDP, sorbitol, sodium azide, *N*-ethylmaleimide, β-mercaptoethanol, *o*-dianisidine, glucose oxidase, peroxidase, Triton X-100, and NP-40 were from Sigma Aldrich, St. Louis, MO. Formaldehyde, glutaraldehyde, cacodylate, osmium oxide, uranyl acetate, and Spurr resin were obtained from EM Sciences, Ft. Washington, PA. Fluorescein isothiocyanate (FITC)–conjugated donkey anti–rabbit and tetramethyl rhodamine isothiocyanate (TRIC)–conjugated donkey anti–mouse secondary antibodies were obtained from Jackson ImmunoResearch Laboratories, West Grove, PA. Fluorsave Reagent was obtained from Calbiochem, San Diego, CA. Secondary antibodies for the Odyssey Imaging System are from LI-COR Biosciences, Lincoln, NE, and Molecular Probes, Eugene, OR. The TNT translation system is from Promega, Madison, WI, and the S-35 methionine and I-125 Protein A from Perkin Elmer, Boston, MA. His-Select HF-Nickel Affinity Gel is from Sigma. IgG Sepharose 6 Fast Flow, Glutathione Sepharose 4B, Protein A Sepharose, and Precision Protease are from GE Healthcare, Milwaukee, WI.

Genetic techniques

The strategy for obtaining mutations in the *MYO2* IQ region for in vitro binding mutations in the individual IQ motifs of *MYO2* used for in vitro binding experiments was generated by two-step fusion PCR. In the first step, two PCR fragments were generated (using pB695 as a template) that shared overlapping sequences at the site of the mutation. Fusion PCR generated a fragment spanning animo acids 925–990 of *MYO2*, which contained the point mutations at the site of fusion. Myo2 mutations in both IQ1 and IQ5 domains were generated by using DNA containing the *myo2-iq1* mutation as a template for the two-step fusion PCR mentioned above.

Strategy for obtaining mutations in the *MYO2* IQ region for yeast transformation

MYO2 mutations in each individual IQ motif for yeast transformation were generated by two-step fusion PCR. In the first step we used genomic DNA to generate two PCR fragments that shared overlapping sequences at the site of the mutation. These fragments were then combined in a fusion PCR reaction with external primers that would allow the formation of a *Bam*HI-*Eco*RI fragment, which was subcloned into the *Bam*HI-*Eco*RI sites of the *MYO2* construct (pB1486). This construct was then used to generate the PCR fragments containing the IQ mutations for integration into yeast.

Introducing point mutations into chromosomal *MYO2*

Yeast strains containing alanine substitutions in one or two IQ motifs of chromosomal *MYO2* were generated using a two-step strategy. In the first step a diploid yeast strain containing a copy of *myo2-Δ6IQ* marked with natR was generated (BY2250). This was obtained by transformation and homologous recombination of PCR fragments containing *myo2-Δ6IQ* and the selectable marker natR into a wild-type diploid strain. External sequences annealed with 651 base pairs upstream of the chromosomal *MYO2* IQ site and 48 base pairs downstream of the *MYO2* open reading frame. Overlapping sequences between the PCR products directed natR 200 base pairs downstream of the *myo2-Δ6IQ* coding sequence. Diploids containing a copy of *myo2-Δ6IQ* showed resistance to clonNAT and the presence of a truncated *myo2-Δ6IQ* protein by Western blot analysis. Diploids containing *myo2-Δ6IQ* were transformed with PCR DNA containing wild-type or mutant iq and the selectable marker kanR. Homologous recombination allowed the substitution of *myo2-Δ6IQ* marked by natR with wild-type or iq mutant marked by kanR. Overlapping sequences between the transforming PCR fragments directed the kanR 100 base pairs downstream of the open reading frame of wild-type or iq mutant. External sequences directed homologous integration 651 base pairs upstream of the IQ site of *myo2-Δ6IQ* and 48 base pairs downstream of the *myo2-6Δ IQ* open reading frame. Diploids were analyzed on plates for loss of natR and gain of kanR resistance and by Western blot analysis for loss of the truncated form of *myo2-Δ6IQ* and gain of full-length Myo2. Diploids were sporulated to generate haploid wild-type and *myo2-iq* mutant strains. Genomic DNA was extracted from all strains to confirm the presence of the desired mutations by sequence analysis.

MYO2 or *MYO2-Δ6IQ* fragments for yeast transformation were generated by fusion PCR from pB694 and pB1176 to obtain *MYO2* and *myo2-Δ6IQ* containing 651 base pairs upstream and 880 base pairs downstream of the IQ site and genomic DNA to obtain *MYO2* containing 810 base pairs downstream of the IQ site and 200 base pairs downstream of the last codon. Fusion PCR generated the required fragments for yeast transformation.

Recombinant proteins

ProtA-Sro7, GST-Sec9, and GST-Myo2IQ were obtained as described previously (Gangar *et al.*, 2005). GST-Mlc1 was purified as described previously for GST fusion proteins (Rossi *et al.*, 1997). Soluble Myo2-IQ (782–990) and Myo2-IQ1,5 proteins were obtained by precision protease cleavage of the GST fusion proteins bound to glutathione Sepharose beads using the manufacturer's (GE Healthcare Milwaukee, WI) protocol.

In vitro binding assays

Radiolabeled Myo2 (782–990), Myo2 (782–925), Myo2 (871–1204), and Myo-IQ1,5 (782–990) with mutant IQ motifs Sro7 (1–1033), Sro7-Δ(3–51), and Sro7-Δ(4–18) were obtained by in vitro transcription and translation of PCR fragments using TNT T7 Quick Master Mix in the presence of S-35 methionine. Binding reactions were set up as previously described (Gangar *et al.*, 2005), except the radiolabeled proteins were incubated with proASro7 bound to IgG beads (1 μM) or GST-Mlc1, GST-Sec9, or GST-Myo2IQ bound to glutathione beads (1 μM). Control beads included ProtA bound to IgG Sepharose (1 μM) and GST bound to glutathione Sepharose (1 μM). PCR conditions for the generation of the radiolabeled proteins were altered to make sure that similar amounts of wild-type and mutant proteins were translated. Binding assays with purified Sro7 to GST-Sec4 were done as described previously (Grosshans *et al.*, 2006).

Plasmid construction

1XGFPSRO7 (pB1270) was generated by introducing *SRO7* (3–1033) obtained from genomic DNA into a plasmid containing the *SRO7* promoter region with *1XGFP* (pB1261) as a *Bam*HI-*Sal*I fragment. *3XGFPSRO7* (pB1564) was generated by inserting a *2XGFP* fragment (from pB1242) as a *Bgl*II-*Bam*HI site into the *Bam*HI site of PB1270. *SRO7* in a *CEN* (*LEU2*) plasmid (pB1763) was generated by transformation of BY1839 with a PCR-generated fragment containing the *LEU2* marker. *3XGFPSRO7* (Δ1–18) was generated by introducing *SRO7* (18–1033) obtained by PCR using oligos containing the truncation into the *Bam*HI-*Sal*I site of *3XGFPSRO7* (pB1564). GST-Mlc1 was generated by subcloning *MLC1* (1–150) obtained from genomic DNA into pGEX4T1 as a *Bam*HI-*Sal*I fragment. GST-Myo2-IQ (782–990) and GST-Myo2-IQ1,5 were subcloned into pGEX6P-1 as *Bam*HI-*Sal*I fragments. *MYO1IQ* (761–932) was obtained by PCR using genomic DNA as a template. *SEC15* under regulation by the tetracycline promoter (pB1816) was generated by subcloning *SEC15* (1–910) obtained from genomic DNA into pCM189 as a *Bam*HI-*Not*I fragment. *SRO7* (Δ4–18) under regulation of the tetracycline promoter (pB1947) was generated by subcloning

SRO7 (Δ4–18) obtained by PCR using oligos containing the deletion as a *Bam*HI-*Not*I fragment in pCM189. *SRO7* under regulation of the galactose-inducible promoter (pB1561) was obtained by subcloning *SRO7* (1–1033) obtained from genomic DNA into pNB527 as a *Bam*HI-*Hin*dIII fragment. *SEC15* under regulation of the galactose-inducible promoter was obtained by subcloning *SEC15* (1–910) obtained from genomic DNA into pNB527 as a *Bam*HI-*Hin*dIII fragment.

Bgl2 and invertase assays

Wild-type and mutant *myo2iq-1,5* and *sec4-P48* mutants were grown overnight to midlog phase in YPD at the permissive temperature of 32°C. Samples for the Bgl2 and invertase assays were taken before and after an 8-h shift to the restrictive temperature of 25°C and processed as described previously (Adamo *et al.*, 1999)

Growth conditions for fluorescence and electron microscopy

The *myo2iq-1,5* mutant cells expressing Sro7 from a tetracycline-regulatable promoter were grown to midlog in selective media at the permissive temperature of 32°C in the presence of doxycycline (1 mg/l) and then shifted to the restrictive temperature of 25°C in selective media in the absence of doxycycline for 8 h before being processed for microscopy.

Wild-type strains expressing Sro7 or Sec15 from the galactose-inducible promoter were grown in raffinose (3%) to midlog and then induced for 10 h with galactose (1%) before fixing and processing for microscopy. All samples were treated as previously described (Adamo *et al.*, 1999).

Fluorescence and immunofluorescence microscopy

All strains analyzed were grown overnight to midlog in selective media, shifted into fresh media for one generation of growth or shifted to restrictive conditions, and then fixed and processed as described previously (Brennwald and Novick, 1993; Roumanie *et al.*, 2005). GFP and RFP fluorescence was detected using MetaMorph software. Immunofluorescence was conducted using monoclonal mouse anti-Sec4 (1:100 dilution) and affinity-purified polyclonal rabbit anti-Sro7 and anti-Sec15 antibodies (1:100 dilution). TRIC-conjugated donkey anti–mouse secondary antibodies were used to detect Sec4 (1:100 dilution), and FITC-conjugated donkey anti–rabbit (1:100 dilution) secondary antibodies were used to detect Sro7 and Sec15 (1:100 dilution).

Immunoprecipitations

Immunoprecipitations from detergent lysates with anti-Sro7 and anti-Myo2 antibodies were performed as described previously (Gangar *et al.*, 2005).

ACKNOWLEDGMENTS

We thank Hal Meekal for expertise with the electron microscope; Ruth Collins, Erfei Bi, Trisha Davis, Lois Weisman, and Laura Shenkman for plasmids; Hao Wu, Leah Watson, and Kelly Watson for critical reading of the manuscript; and Kelly Watson and Mallory Demonch for assistance in generating plasmids and reagents utilized in this work. This work was supported by grants from the National Institutes of Health (GM-54712) and the G. Harold and Leila Y. Mathers Foundation.

REFERENCES

Adamo JE, Rossi G, Brennwald P (1999). The Rho GTPase Rho3 has a direct role in exocytosis that is distinct from its role in actin polarity. Mol Biol Cell 10, 4121–4133.

Adamo JE, Moskow JJ, Gladfelter AS, Viterbo D, Lew DJ, Brennwald PJ (2001). Yeast Cdc42 functions at a late step in exocytosis, specifically during polarized growth of the emerging bud. J Cell Biol 155, 581–592.

Bähler M, Rhoads A (2002). Calmodulin signaling via the IQ motif. FEBS Lett 513, 107–113.

Beningo KA, Lillie SH, Brown SS (2000). The yeast kinesin-related protein Smy1p exerts its effects on the class V myosin Myo2 via a physical interaction. Mol Biol Cell 11, 691–702.

Boyd C, Hughes T, Pypaert M, Novick P (2004). Vesicles carry most exocyst subunits to exocytic sites marked by the remaining two subunits, Sec3p and Exo70p. J Cell Biol 167, 889–901.

Brennwald P, Novick P (1993). Interactions of three domains distinguishing the Ras-related GTP-binding proteins Ypt1 and Sec4. Nature 362, 560–563.

Brennwald P, Kearns B, Champion K, Keränen S, Bankaitis V, Novick P (1994). Sec9 is a SNAP-25-like component of a yeast SNARE complex that may be the effector of Sec4 function in exocytosis. Cell 79, 245–258.

Catlett NL, Weisman LS (1998). The terminal tail region of a yeast myosin-V mediates its attachment to vacuole membranes and sites of polarized growth. Proc Natl Acad Sci USA 95, 14799–14804.

Elkind NB, Walch-Solimena C, Novick PJ (2000). The role of the COOH terminus of Sec2p in the transport of post-Golgi vesicles. J Cell Biol 149, 95–110.

Gangar A, Rossi G, Andreeva A, Hales R, Brennwald P (2005). Structurally conserved interaction of Lgl family with SNAREs is critical to their cellular function. Curr Biol 15, 1136–1142.

Goud B, Salminen A, Walworth NC, Novick PJ (1988). A GTP-binding protein required for secretion rapidly associates with secretory vesicles and the plasma membrane in yeast. Cell 53, 753–768.

Govindan B, Bowser R, Novick P (1995). The role of Myo2, a yeast class V myosin, in vesicular transport. J Cell Biol 128, 1055–1068.

Grosshans BL, Andreeva A, Gangar A, Niessen S, Yates JR III, Brennwald P, Novick P (2006). The yeast lgl family member Sro7 is an effector of the secretory Rab GTPase Sec4p. J Cell Biol 172, 55–66.

Grosshans BL, Ortiz D, Novick P (2006). Rabs and their effectors: achieving specificity in membrane traffic. Proc Natl Acad Sci USA 103, 11821–11827.

Guo W, Roth D, Walch-Solimena C, Novick P (1999). The exocyst is an effector for Sec4p, targeting secretory vesicles to sites of exocytosis. EMBO J 18, 1071–1080.

Hattendorf DA, Andreeva A, Gangar A, Brennwald PJ, Weis WI (2007). Structure of the yeast polarity protein Sro7 reveals a SNARE regulatory mechanism. Nature 446, 567–571.

Johnston GC, Prendergast JA, Singer RA (1991). The *S. cerevisiae MYO2* gene encodes an essential myosin for vectorial transport of vesicles. J Cell Biol 113, 539–551.

Kagami M, Toh-e A, Matsui Y (1998). Sro7p, a *Saccharomyces cerevisiae* counterpart of the tumor suppressor l(2)gl protein, is related to myosins in function. Genetics 149, 1717–1727.

Kogel T, Rudolf R, Hodneland E, Hellwig A, Kuznetsov SA, Seiler F, Sollner TH, Barroso J, Gerdes HH (2010). Distinct roles of myosin Va in membrane remodeling and exocytosis of secretory granules. Traffic 11, 637–650.

Krendel M, Mooseker MS (2005). Myosins: tails (and heads) of functional diversity. Physiology 20, 239–251.

Larsson K, Bohl F, Sjostrom I, Akhtar N, Strand D, Mechler BM, Grabowski R, Adler L (1998). The *Saccharomyces cerevisiae SOP1* and *SOP2* genes, which act in cation homeostasis, can be functionally substituted by the *Drosophila lethal(2)giant larvae* tumor suppressor gene. J Biol Chem 273, 33610–33618.

Lehman K, Rossi G, Adamo JE, Brennwald P (1999). Yeast homologues of tomosyn and lethal giant larvae function in exocytosis and are associated with the plasma membrane SNARE, Sec9. J Cell Biol 146, 125–140.

Li Z, Sacks DA (2003). Elucidation of the interaction of calmodulin with the IQ motifs of IQGAP1. J Biol Chem 278, 4347–4352.

Lipatova Z, Tokarev AA, Jin Y, Mulholland J, Weisman LS, Segev N (2008). Direct interaction between a myosin V motor and the Rab GTPases Ypt31/32 is required for polarized secretion. Mol Biol Cell 10, 4177–4187.

Markgraf DF, Ahnert F, Arlt H, Mari M, Peplowska K, Epp N, Griffith J, Reggiori F, Ungermann C (2009). The CORVET subunit Vps8 cooperates with the Rab5 homolog Vps21 to induce clustering of the late endosomal compartments. Mol Biol Cell 20, 5276–5289.

Ohya T, Miaczynska M, Coskun U, Lommer B, Runge A, Drechsel D, Kalaidzidis Y, Zerial M (2009). Reconstitution of Rab- and

SNARE-dependent membrane fusion by synthetic endosomes. Nature 459, 1091–1097.
Ortiz D, Medkova M, Walch-Solimena C, Novick P (2002). Ypt32 recruits the Sec4p guanine nucleotide exchange factor, Sec2p, to secretory vesicles; evidence for a Rab cascade in yeast. J Cell Biol 157, 1005–1015.
Peng CY, Manning L, Albertson R, Doe CQ (2000). The tumour-suppressor genes *lgl* and *dlg* regulate basal protein targeting in *Drosophila* neuroblasts. Nature 408, 596–600.
Pfeffer SR (1999). Transport-vesicle targeting: tethers before SNAREs. Nature Cell Biol 1, E17–E22.
Pruyne DW, Schott DH, Bretscher A (1998). Tropomyosin-containing actin cables direct the Myo2p-dependent polarized delivery of secretory vesicles in budding yeast. J Cell Biol 143, 1931–1945.
Rossi G, Salminen A, Rice LM, Brünger AT, Brennwald P (1997). Analysis of a yeast SNARE complex reveals remarkable similarity to the neuronal SNARE complex and a novel function for the C-terminus of the SNAP-25 homolog, Sec9. J Biol Chem 272, 16610–16617.
Roumanie O, Wu H, Molk JN, Rossi G, Bloom K, Brennwald P (2005). Rho GTPase regulation of exocytosis in yeast is independent of GTP hydrolysis and polarization of the exocyst complex. J Cell Biol 170, 583–594.
Salminen A, Novick PJ (1989). The Sec15 protein responds to the function of the GTP binding protein, Sec4, to control vesicular traffic in yeast. J Cell Biol 109, 1023–1036.
Schott D, Ho J, Pruyne D, Bretscher A (1999). The COOH-terminal domain of Myo2p, a yeast myosin V, has a direct role in secretory vesicle targeting. J Cell Biol 147, 791–808.
Schott DH, Collins RN, Bretscher A (2002). Secretory vesicle transport velocity in living cells depends on the myosin-V lever arm length. J Cell Biol 156, 35–39.
Segev N (2001). Ypt/Rab GTPases: regulators of protein trafficking. Sci STKE 100, re11.
Spang A (2004). Vesicle transport: a close collaboration of Rabs and effectors. Curr Biol 14, R33–R34.
Stevens RC, Davis TN (1998). Mlc1p is a light chain for the unconventional myosin Myo2p in *Saccharomyces cerevisiae*. J Cell Biol 142, 711–722.
TerBush DR, Maurice T, Roth D, Novick PJ (1996). The exocyst is a multiprotein complex required for exocytosis in *Saccharomyces cerevisiae*. EMBO J 15, 6483–6494.
Vale RD (2003). The molecular motor toolbox for intracellular transport. Cell 112, 467–480.
Wadskog I, Maldener C, Proksch A, Madeo F, Adler L (2004). Yeast lacking the SRO7/SOP1-encoded tumor suppressor homologue show increased susceptibility to apoptosis-like cell death on exposure to NaCl stress. Mol Biol Cell 15, 1436–1444.
Walch-Solimena C, Collins RN, Novick PJ (1997). Sec2p mediates nucleotide exchange on Sec4p and is involved in polarized delivery of post-Golgi vesicles. J Cell Biol 137, 1495–1509.
Yamamoto H, Koga H, Katoh Y, Takahashi S, Nakayama K, Shin HW (2010). Functional crosstalk between Rab14 and Rab4 though a dual effector, RUFY1/Rabip4. Mol Biol Cell 21, 2746–2755.
Zhang X, Wang P, Gangar A, Zhang J, Brennwald P, Terbush D, Guo W (2005). Lethal giant larvae proteins interact with the exocyst complex and are involved in polarized exocytosis. J Cell Biol 170, 273–283.